Chapter IV *Expanded skeletal stem and progenitor cells promote and participate in induced bone regeneration at subcritical BMP-2 dose*

Manuscript submitted to Biomaterials

Expanded skeletal stem and progenitor cells promote and participate in induced bone regeneration at subcritical BMP-2 dose

Panagiota Papageorgiou[1], Queralt Vallmajo-Martin[1], Malgorzata Kisielow[2], Esther Kleiner[1], Martin Ehrbar[1]*

Affiliations:

[1] Department of Obstetrics, University Hospital Zurich, University of Zurich, Schmelzbergstr. 12, 8091 Zurich, Switzerland.

[2] Flow Cytometry Core Facility, ETH Zurich, Otto-Stern-Weg 7, 8093 Zurich, Switzerland.

* Correspondence should be addressed to Martin Ehrbar: martin.ehrbar@usz.ch

Abstract

The regeneration of large bone defects remains an unsolved clinical problem, which could benefit from recent findings on the biology of skeletal stem and progenitor cells. The elucidation of conditions to specifically control their dynamic and function will likely enable the development of novel treatment strategies. In this study, we aimed at dissecting the role of skeletal stem and progenitor cell recruitment and osteogenic cues in biomaterials-assisted bone regeneration. We show that bone morphogenetic protein (BMP)-2 dose-dependently promoted the enrichment of both skeletal stem (SSCs) and bone cartilage stromal progenitor cells (BCSPs) within biomaterials treated at healing bone defects sites. Furthermore, we demonstrate that prospectively isolated neonatal bone derived, as well as culture expanded SSCs and BCSPs differentiate into osteogenic cells and potentiate the bone-healing efficacy of BMP-2 treatment. These results indicate that growth factor releasing materials should be designed to first augment the number of SSCs and BCSPs, followed by their osteogenic differentiation to potentiate the healing of bone defects. Additionally, we demonstrate that culture expanded SSCs and BCSPs are easily accessible cell sources that allow the study of novel bone healing regimen under controlled *in vitro* and *in vivo* conditions.

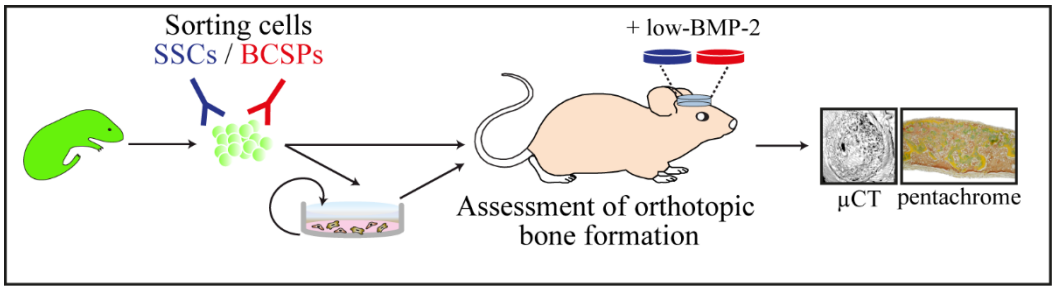

Keywords: Skeletal Stem Cells, Bone Cartilage Stromal Progenitors, TGPEG hydrogel, low dose, BMP-2, orthotopic bone formation.

Introduction

While BMP-2 has been demonstrated to significantly induce bone regeneration in human patients, the complication profile, related to the supraphysiologic dose of BMP-2 delivered in current formulations (1.5mg/cm^3), has led to safety concerns that currently limit its clinical use (*1, 2*). Reported complications include early inflammatory reaction and osteolysis, ectopic bone formation and a possible increase in the risk of malignancy (*3*). On the other hand, previously described clinical studies, based on strategies promoting the inherent (limited) capacity of bone to regenerate, have been a strong stimulus for the development of alternative approaches to bone regeneration (*4-8*).

Although mesenchymal stem/progenitor cells are very promising tools for enhancing bone regeneration, showing statistically significant efficacy in clinical trials, they remain difficult to be implemented (*9, 10*). This is most likely due to still lacking strict definition of stem/progenitor cell selection criteria and because the cells' regenerative capability cannot readily be controlled once transplanted (*11, 12*). Currently evaluated strategies to promote better or faster healing consist of delivering osteoinductive growth factors and/or stem/progenitor cells through osteoconductive natural or engineered biomimetic biomaterials (*13, 14*). While natural biomaterials such as collagen or fibrin hydrogels are excellent cell substrates, their inherent biological properties are responsible for limited control over *in vivo* stability and provision of matrix-catenated or soluble signaling cues (*15, 16*). To overcome these limitations in recent years multiple semisynthetic (*17*) and fully synthetic biomaterials have been developed (*18*). By the use of biomaterials building blocks with increasingly defined chemical, physical and biological properties, biomaterials with almost independently controllable stiffness, degradability, cell-adhesive functions and growth factor affinities are now becoming available (*19*). These materials offer the great advantage of being tailorable towards the transplantation of cells with regenerative capacity as well as the delivery of potential healing and regeneration governing signals that enable the induction and morphogenesis of functional tissues (*20, 21*).

The healing of bone defects is a complex process, involving multiple cellular and molecular mechanisms (*5, 6*). Among the cells, which are currently suggested to control the early healing environment are neutrophils and macrophages, which by releasing growth factors and secreting cytokines, can actively promote the induction and

mobilization of cells with bone forming capacity (*22-25*). Although in recent years important insights into phenotypic properties and anatomical localization of human and murine bone forming stem and progenitor cells have been obtained, the functional relation of differently characterized cell populations remains elusive (*26-28*). Furthermore, their participation in bone healing, as well as signals responsible for their induction and mobilization, need further characterization (*29-31*). Recently, Chan et al. provided evidence that BMP-2 delivery in extra-skeletal regions, such as subcutaneous sites and renal capsule, can induce the *de novo* formation of skeletal stem cells (SSCs) ($CD45^-TER119^-Tie2^-AlphaV^+Thy^-6C3^-CD105^-CD200^+$). They further suggested that skeletogenesis, similar to haematopoiesis, may proceed through a developmental hierarchy of lineage-restricted progenitors with distinct cell-surface marker profiles and skeletal tissue fates (*32*). In this model SSCs initiate skeletogenesis by giving rise to increasingly fate restricted progenitors, bone cartilage stromal progenitors (BCSPs) ($CD45^-TER119^-Tie2^-AlphaV^+Thy^-6C3^-CD105^+$) that promote the spontaneous formation of bone, cartilage, and bone marrow upon *in vivo* transplantation. To enable the translation of the newly acquired knowledge on the skeletal stem and progenitor cells it will be important to characterize and dissect factors leading to their induction, recruitment, expansion as well as osteogenic differentiation and integrate them into novel biomaterials. Therefore, the aim of this study was to understand whether subcritical, biomaterials-delivered, concentrations of BMP-2 are able to increase the number of SSCs and BCSPs and if these cells are able to differentiate into bone forming cells.

In previous studies of our laboratory an enzymatically formed modular designed, biomimetic PEG-based biomaterial (*33, 34*) was employed to treat critical-sized murine calvarial defects. These fully defined biodegradable biomaterials were readily replaced by bone tissue when high-dose of BMP-2 was incorporated (*35, 36*). Consequently, we reasoned that this, on a blank slate-based rationally designed, biomaterial would be the ideal system to specifically study the contribution of osteogenic signals and stem/progenitor cells to bone healing. Our data indicate that expanded SSCs and BCSPs from limbs and sternum of P3 pups can undergo osteogenic differentiation *in vitro.* When transplanted, these subpopulations spontaneously differentiate towards osteogenic lineages and in presence of low-dose BMP-2 participate in the regeneration of bone. Our results suggest that short-term expanded SSCs and BCSPs maintain their osteogenic properties and regenerate bone when applied at a healing fracture site, in murine

calvarial bone. Thus, we propose the use of expanded SSCs and BCSPs in combination with minimal osteoinductive signals to study cellular and molecular bone processes of bone healing and to elucidate healing stimulation signals.

Results

BMP-2-mediated accumulation of SSCs and BCSPs at sites of bone healing

To determine the effect of BMP-2 on the accumulation of stem cells during bone healing, we generated critical-sized (4 mm diameter) defects in calvarial bones of C57Bl/6 mice and treated them with biomimetic hydrogels which contained no, low-dose (0.2µg) or high-dose (1µg) of BMP-2 (**Figure 1A**). Previously, we have reported that murine bone matrix deposition is initiated 1 week after treatment with BMP-2 fast-releasing biomimetic hydrogels (*35*), elsewhere it was shown that expansion of SSCs and BSCPs was most extensive during spontaneous bone healing at the stage of callus formation (*40, 41*). Therefore, to determine the number of SSCs and BCSPs participating in these early stages of healing hydrogel implants were retrieved 8 days post treatment. Implant-trapped cells were enzymatically released and characterized by flow cytometry based on the absence of haematopoietic and endothelial markers (CD45, Ter-119, Tie-2), the presence of the osteoblastic marker (AlphaV), as well as, the differential expression of Thy, 6C3, CD105 and CD200 (*32, 42*). While in the control implants the subset of $CD45^-TER119^-Tie2^-Thy^-6C3^-$ comprised 0.93 ± 0.33 % of all nucleated cells, SSCs ($CD45^-TER119^-Tie2^-AlphaV^+Thy^-6C3^-CD105^-CD200^+$) as well as BCSPs ($CD45^-TER119^-Tie2^-AlphaV^+Thy^-6C3^-CD105^+$) were almost absent, comprising 0.013 ± 0.005 % and 0.017 ± 0.017 % respectively (**Figure 1B** and **C**). Upon treatment with low-dose and high-dose BMP-2 the number of the negative subset increased to 2.08 ± 0.36 % and 5.74 ± 0.66 %, respectively. Importantly, upon treatment with low-dose BMP-2 the fraction of both SSCs and BCSPs significantly increased to 0.18 ± 0.007 % and 0.14 ± 0.009 %, respectively. Moreover, in presence of high-dose BMP-2, the fraction of both SSCs and BCSPs was even further enhanced to 1.71 ± 0.23 % and 0.4 ± 0.59 %, respectively. While hydrogels containing no or low-dose BMP-2 did not support bone regeneration, high-dose BMP-2 resulted in the efficient closure of bone defects after 4 weeks of treatment (**Figure 1D**). These results demonstrate that hydrogel-delivered BMP-2 promoted the number of endogenous, healing-associated SSCs and BCSPs in a dose dependent manner.

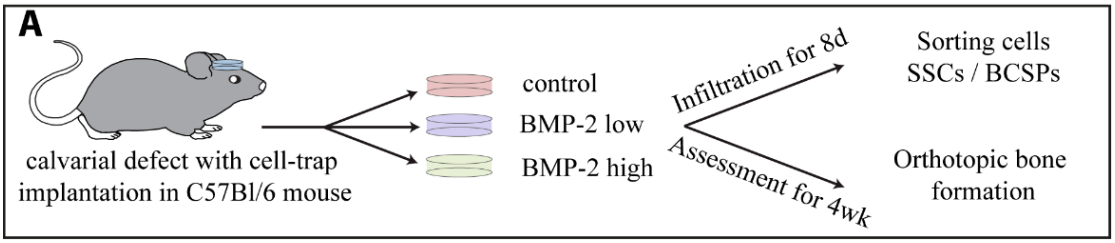
A
calvarial defect with cell-trap
implantation in C57Bl/6 mouse
control
BMP-2 low
BMP-2 high
Infiltration for 8d
Assessment for 4wk
Sorting cells
SSCs / BCSPs
Orthotopic bone
formation

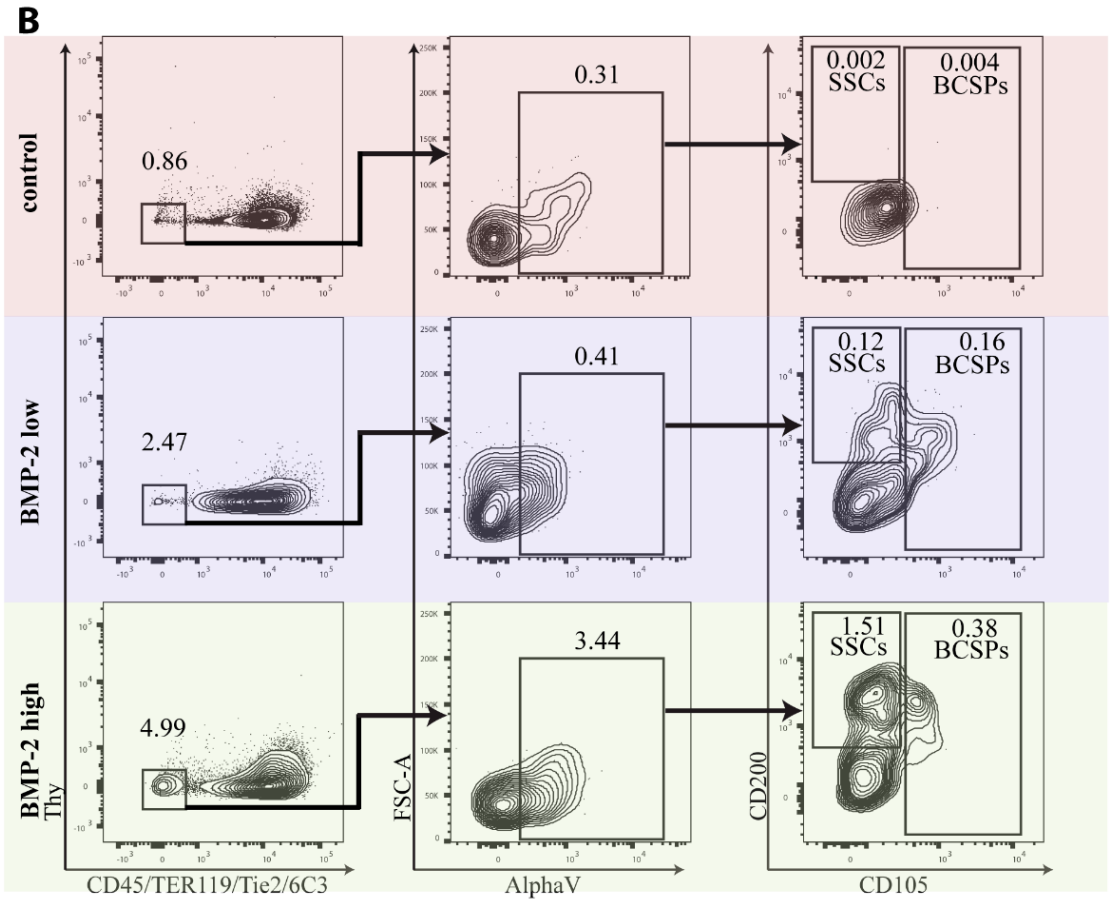
B
control
BMP-2 low
BMP-2 high
0.86
0.31
0.002
SSCs
0.004
BCSPs
2.47
0.41
0.12
SSCs
0.16
BCSPs
4.99
3.44
1.51
SSCs
0.38
BCSPs
Thy
FSC-A
CD200
CD45/TER119/Tie2/6C3
AlphaV
CD105

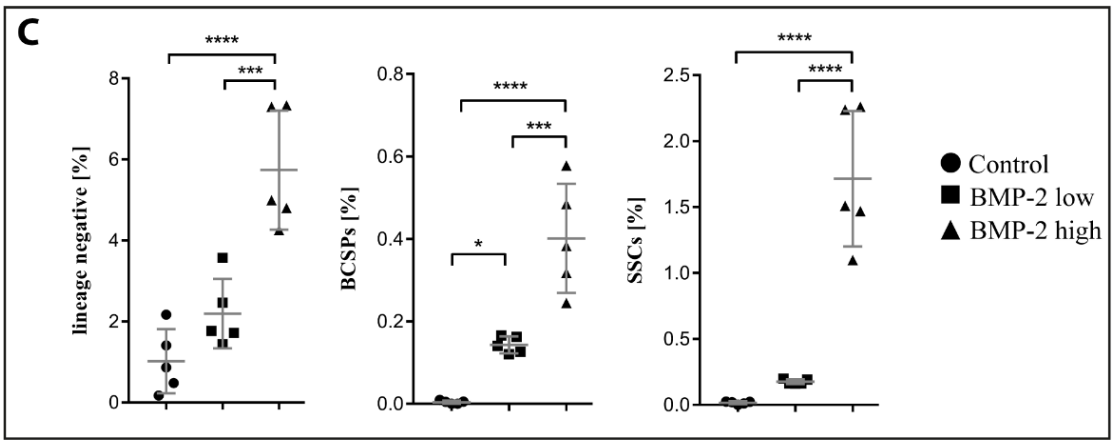
C
lineage negative [%]
BCSPs [%]
SSCs [%]
Control
BMP-2 low
BMP-2 high

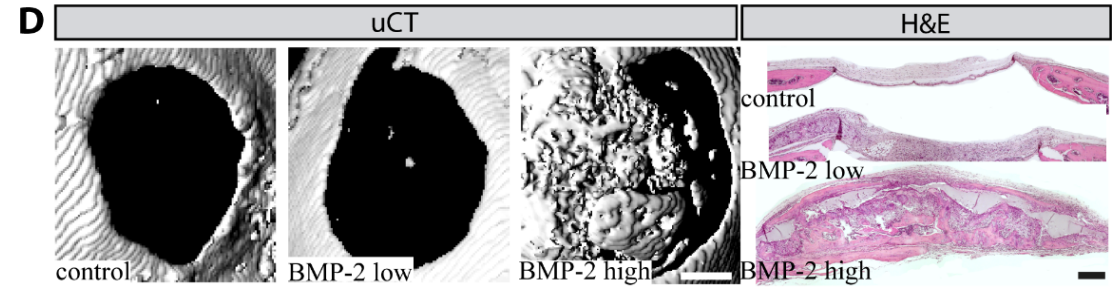
D
uCT
H&E
control
BMP-2 low
BMP-2 high
control
BMP-2 low
BMP-2 high

Figure 1. SSC and BCSP recruitment into TGPEG hydrogels during fracture healing. (A) TG-PEG hydrogels containing 0, 0.2µg and 1µg BMP-2 were implanted in murine critical-size calvarial defects. Fractions of infiltrating SSCs and BCSPs were determined by flow cytometry of enzymatically harvested cells from day 8 implants. Bone formation was assessed at 4weeks by µCT. **(B)** Representative FACS strategy on pre-gated live singlet cells is shown. **(C)** Quantitative assessment of recruited injury-associated SSCs and BCSPs. Data is depicted as mean ± SD, n = 5. One-way ANOVA Bonferroni's post hoc test * $p < 0.05$, ** $p < 0.01$ *** $p < 0.001$, **** $p < 0.0001$. **(D)** Representative top views of 3D surface rendered µCT measurements for the different doses of BMP-2 (scale bar: 1 mm) and representative histological evaluations (scale bar: 200µm).

In vivo osteogenic potential of prospectively isolated SSCs and BCSPs

SSCs and BCSPs were shown to be involved in BMP-2 mediated healing of bone as well as in neonatal bone formation, indicating that in both processes they could have equivalent functions (*32*, *40*). Therefore, we reasoned that to obtain higher numbers of the low-abundant SSCs and BCSPs for further *in vitro* and *in vivo* evaluations these cells could be isolated from limbs and sternum of P3 GFP-mice (mice express enhanced Green Fluorescent Protein under direction of the human ubiqutin C promoter) as earlier described by (*32, 40, 42*) (**Figure 2A** and **S1**). When seeded at clonal dilution of 110 cells cm^{-2} for 9 days both prospectively isolated cell fractions formed fibroblast colony forming units (CFU-F), which however were significantly higher for SSCs as compared to BCSPs (**Figure 2B**). Both subpopulations showed spindle-shaped morphology (**Figure 2B**) and had strong proliferative potential.

Previous studies have demonstrated that SSCs and BCSPs spontaneously form bone when implanted beneath the renal capsule (*32, 40, 42*). Here, to determine their spontaneous osteogenic differentiation in a healing bone microenvironment prospectively isolated, non-expanded SSCs and BCSPs were encapsulated in biomimetic hydrogel discs (4.4 mm diameter, 0.8 mm thickness) and transplanted into segmental bone defects (**Figure 2A**). Even though SSCs are about 33-fold less abundant (8.98%) than BCSPs (42.1 %) (**Figure S1**) we were able to transplant prospectively isolated SSCs at densities of 10^5 cells mL^{-1} / hydrogel (**Figure S2**). While these low cellular densities of SSCs were unable to substantially support the global healing of critical-sized bone defects, micro computed tomography (µCT) as well as histological evaluations showed that small bony particles were formed (**Figure S2**). Examination of decalcified tissue sections, stained with pentachrome or immunohistochemically using a GFP-specific antibody, showed that transplanted prospectively isolated SSCs spontaneously differentiated into both osteoblasts and osteocytes arranged in small bone nodules. Comparably, transplanted BCSPs (10^6 cells mL^{-1} / hydrogel) contributed to the formation of bony ossicles but were

insufficient to stimulate significant bone healing. In contrast, co-treatments with low-dose BMP-2 and BCSPs elicited a robust bone formation leading to a continuous shell of mineralized bone covering the defect as illustrated and quantified by μCT (**Figure 2C**). Examination of tissue sections revealed that the bone cortex encompassed trabecular bone elements as well as a haematopoietic compartment. Pentachrome and GFP-specific stains demonstrated that transplanted BCSPs had differentiated into bone-lining osteoblasts as well as matrix entrapped osteocytes. In contrast, in treatments of low-dose BMP-2 alone signs of bone remodelling at the wound edges were observed, but bone regeneration was completely absent (**Figure 2D**). Together, these data indicate that both SSCs and BCSPs in the bone healing microenvironment could spontaneously differentiate into osteogenic lineage cells. Moreover, in presence of low, but still subcritical dose of BMP-2, BCSPs participated in a robust bone formation.

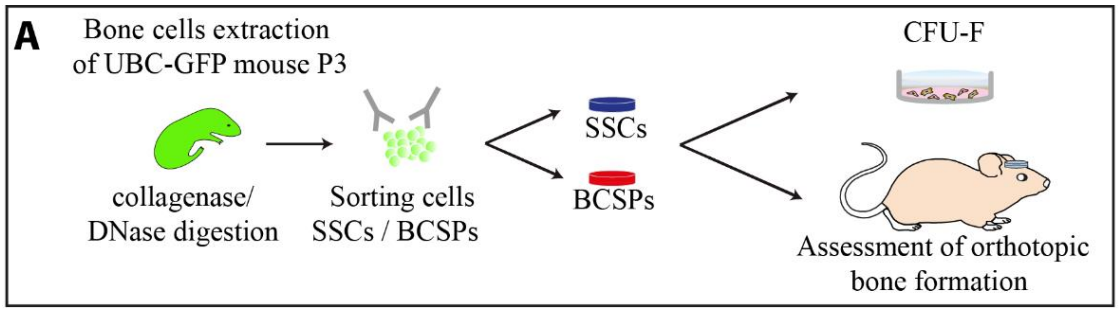
A
Bone cells extraction
of UBC-GFP mouse P3
collagenase/
DNase digestion
Sorting cells
SSCs / BCSPs
SSCs
BCSPs
CFU-F
Assessment of orthotopic
bone formation

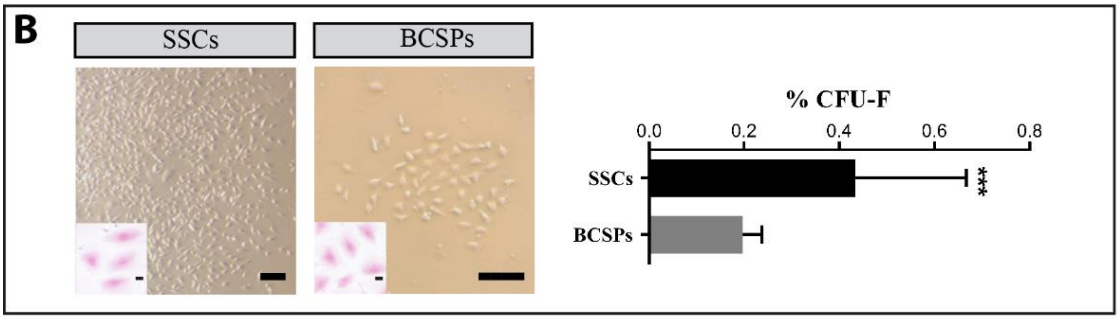
B
SSCs
BCSPs
% CFU-F
0.0
0.2
0.4
0.6
0.8
SSCs
BCSPs
****

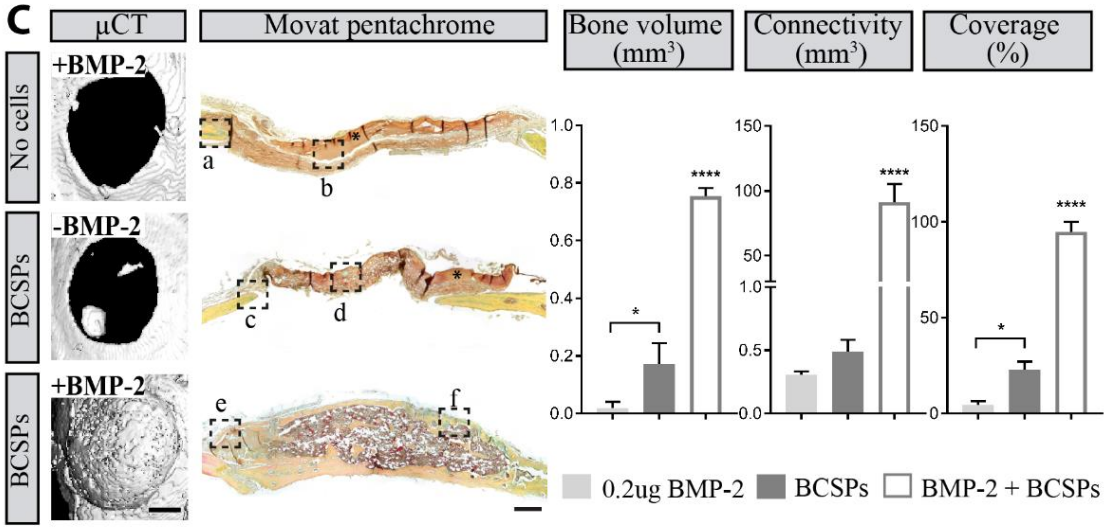
C
µCT
Movat pentachrome
Bone volume (mm³)
Connectivity (mm³)
Coverage (%)
No cells
+BMP-2
BCSPs
-BMP-2
BCSPs
+BMP-2
a
b
c
d
e
f
****
*
0.2ug BMP-2
BCSPs
BMP-2 + BCSPs

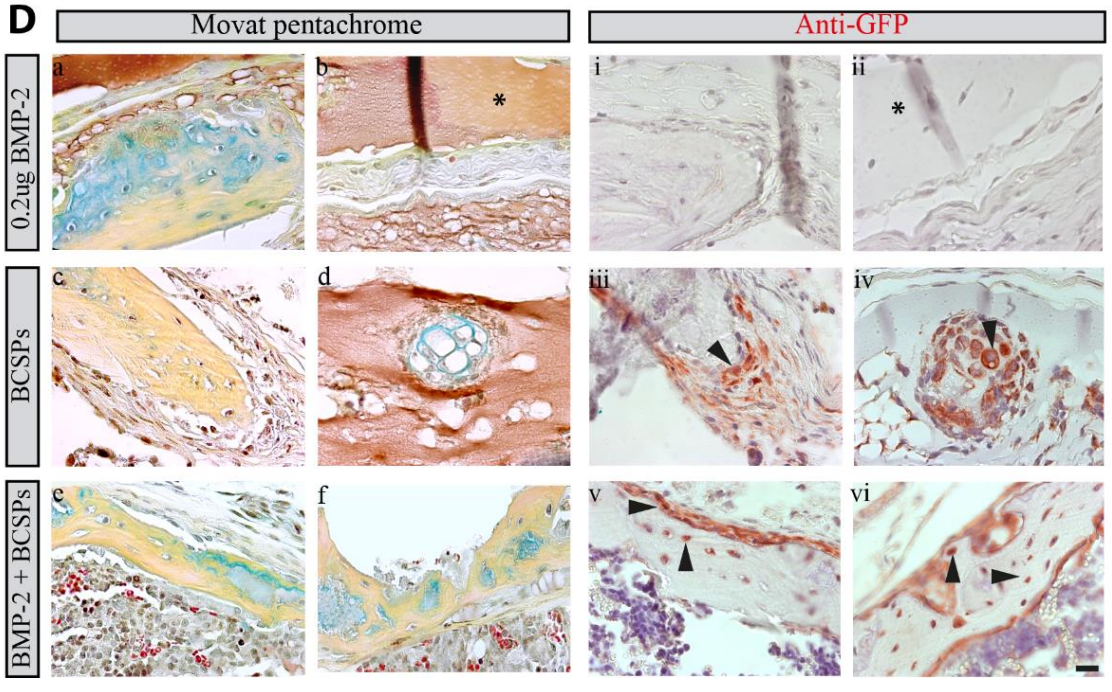
D
Movat pentachrome
Anti-GFP
0.2ug BMP-2
BCSPs
BMP-2 + BCSPs
a
b
c
d
e
f
i
ii
iii
iv
v
vi
*

Figure 2. Characterization of prospectively isolated SSCs and BCSPs. (**A)** SSC and BCSP subpopulations were prospectively isolated from limbs and sternum of P3 GFP^+ mice. Their properties were characterized by *in vitro* colony formation or contribution to the regeneration of calvarial bone defects. **(B)** Representative colonies 4 days after seeding SSCs and BCSPs at a density of 110 cells cm^{-2} by bright field microscopy of unstained (scale bar: 200 µm) and crystal violet stained (inlets, scale bar: 50 µm) cultures. Quantification of generated colonies after 9 days of culture. Data is depicted as mean ± SD, SSCs = 18, BCSPs = 6. *** $p < 0.001$ (unpaired t-test). **(C)** Healing of calvarial defects in immunocompromised mice 4 weeks after implantation of TGPEG hydrogels containing 0.2µg BMP-2, 10^6 prospectively isolated BCSPs mL^{-1} / hydrogel or combinations thereof. Representative top views of 3D surface rendered µCT measurements are shown (scale bar: 1 mm, left panel) along with Movat pentachrome stained coronal cross sections [scale: 200 µm, middle panel, red (fibrin) indicates muscle/vascularized tissue; yellow (reticular fibers/collagen) indicates bone; green/blue (mucin) indicates cartilaginous tissue; and black, nuclei and elastic fibers]. µCT-based quantitative assessment of generated bone volume, connectivity and % coverage (left panel). Data is depicted as mean ± SD, n = 3. One-way ANOVA Bonferroni's post hoc test * $p < 0.05$, ** $p < 0.01$, *** $p < 0.001$, **** $p < 0.0001$. (**D)** Contribution of BCSPs to newly formed calvarial bone was assessed by immunohistochemistry. **(a-f)** Inlets of coronal cross pentachrore stained sections. **(i-vi)** Anti-GFP specific staining for localization of $BCSPs^+$ in osteocyte position (scale bar: 20 µm, black triangles indicate stained BCSPs in osteocyte position within the remodeling healing area, asterisks indicate the remaining volume of the cell-trap). For the prospectively isolated SSCs see supplementary S2.

Culture expanded SSCs and BCSPs maintain their *in vitro* osteogenic differentiation potential

To further improve the availability of high numbers of hardly accessible SSCs and BCSPs, both cell types were prospectively isolated from neonatal mice and expanded under standard culture conditions. Therefore, to determine how rapid SSCs and BCSPs lose their phenotypic identity in culture, both cellular fractions were expanded for two passages before reanalysis for the cell-surface markers CD105 and CD200 (**Figure S3**). Only 3.7% of expanded SSCs (e-SSCs) expressed CD200 (**Figure S3A**), while 43.3% of the culture-expanded BCSPs (e-BCSPs) remained CD105 positive (**Figure S3B**). Interestingly, 33.7% of the e-SSCs acquired the expression of CD105 while they lost CD200 expression, exhibiting a phenotype comparable to prospectively isolated BCSPs (**Figure S3A**). These data show that both e-SSCs and e-BCSPs rapidly lose their initial marker profile expression and indicate that a potential shift to a more differentiated phenotype could occur upon *in vitro* culture.

To test their *in vitro* osteogenic differentiation potential e-SSCs and e-BCSPs were seeded at a density of 3000 cells cm^{-2} on tissue culture polystyrene (TCP) plates. They were cultured for 8 days in presence or absence of 100 ng mL^{-1} BMP-2 before the expression and activity of alkaline phosphatase (ALP), an intermediate marker of bone formation, was assessed. Isolated murine embryonic fibroblasts (mEFs) served as a negative and mouse pre-osteoblast cell line (MC3T3) as positive controls (**Figure 3A** and **B**). While mEFs and MC3T3 did not show a significant ALP activity under control culture condition, in both SSCs and BCSPs a substantial basal expression and activity of ALP was observed.

To better mimic the differentiation microenvironment present in bone defects, all cell types were exposed to BMP-2 (*43*) resulting in the significant upregulation of ALP in all osteogenic cell types. Interestingly, compared to MC3T3 cells SSCs and BCSPs reached almost 15 and 25-fold higher levels of ALP activity.

We next investigated matrix mineralization, a late parameter of osteogenic differentiation, in an extracellular matrix (ECM) mimicking environment. Therefore, mEFs, BCSPs, SSCs and MC3T3 cells were encapsulated in biomimetic hydrogels and cultured for 14 days under non-osteogenic or osteogenic conditions (supplemented with 100 ng mL^{-1} of BMP-2). While under non-osteogenic conditions mEFs did not show any signs of mineralization, in SSCs, BCSPs and MC3T3 cells, led to increasing numbers of mineralized nodules were observed by Alizarin Red S (ARS) stain (**Figure 3C**). More importantly, when cultured under osteogenic differentiation conditions SSCs and BCSPs significantly increased matrix mineralization in comparison to mEFs and MC3T3 (0.24 ± 0.01 and 0.34 ± 0.03 to 0.01 ± 0.0003 and 0.07 ± 0.005, respectively) cells as shown by ARS stain and absorbance measurements of extracted ARS (**Figure 3C** and **D**).

To further confirm the osteogenic differentiation of 3D cultured cells the mRNA expression levels of the osteogenic markers alkaline phosphatase (ALP) and the transcription factor SP7 (Osterix) were analyzed by qRT-PCR (**Figure 3E** and **F**). In all osteogenic cells, these genes were significantly induced by BMP-2. Notably, the osteogenic marker ALP was significantly increased in the treated SSCs subpopulation confirming the observed results from the measured protein activity levels secreted from the cells. Osterix, which was shown to be required for craniofacial development and participate in the differentiation into mature osteoblasts (*44*), was upregulated significantly in the treated calvarial preosteoblasts MC3T3, as expected, compared to the SSC and BCSP populations, confirming its broader osteolineage-specific expression. Taken together, these data suggest that under standard culture conditions e-SSCs and e-BCSPs maintained their osteogenic properties to a significant degree.

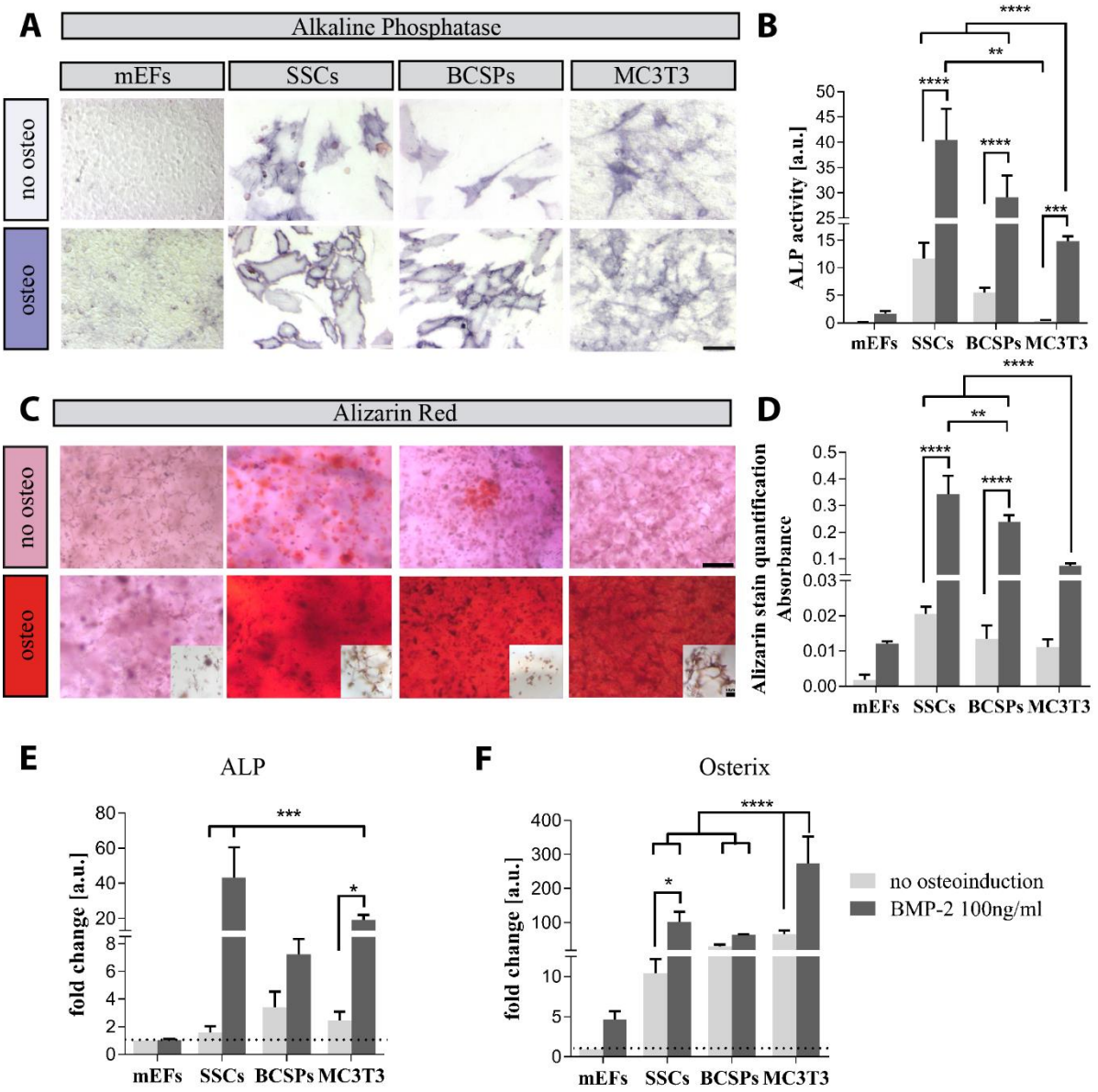

Figure 3. ***In vitro*** **osteogenic ability of expanded SSCs and BCSPs. (A)** The different cell populations were seeded at 3000 cells cm^{-2} density and cultured for 8 days in presence of 0 (no osteoinduction) and 100 ng mL^{-1} BMP-2 (osteoinduction), followed by alkaline phosphatase (ALP) staining (scale bar: 50 µm). **(B)** Quantitative ALP activity assay in corresponding subpopulations. ALP activity values were normalized to DNA content of the samples. **(C)** The different cell populations were encapsulated in TGPEG hydrogels (5 * 10^6 mL^{-1} / hydrogel) and cultured for 14 days in presence or absence of osteogenic differentiation media (scale bar: 200 µm). Inlets represent stained cells entrapped in the hydrogel, followed by alizarin red staining (ARS) staining (scale bar: 50 µm). **(D)** Quantitative ARS by absorbance at 405 nm in corresponding subpopulations. Data is depicted as mean ± SD, n = 4. Two-way ANOVA Bonferroni's post hoc test: * $p < 0.05$, ** $p < 0.01$ *** $p < 0.001$, **** $p < 0.0001$. **(E-F)** Gene expression analysis of early markers of osteogenesis. The different cell populations were encapsulated in TGPEG hydrogels (3 * 10^6 mL^{-1} / hydrogel) and cultured for 8 days in presence of 0 (no osteoinduction) and 100 ng mL^{-1} BMP-2 (osteoinduction). ALP and Osterix genes were upregulated in treated SSCs and BCSPs. Reference gene for all the populations was Actb and the normalization was done upon mEFs. CT values distibution of Actb gene see supplementary S4. Data is depicted as mean ± SD, n = 4. Two-way ANOVA Bonferroni's post hoc test * $p < 0.05$, ** $p < 0.01$ *** $p < 0.001$, **** $p < 0.0001$.

In vivo osteogenic differentiation potential of e-SSCs and e-BCSPs

In vitro differentiation does not sufficiently reproduce *in vivo* microenvironmental conditions and must be confirmed by *in vivo* evaluations (*29*). Therefore, to confirm their osteogenic differentiation potential GFP$^+$ e-SSCs and e-BCSPs were encapsulated (10^6 cells mL^{-1}/ hydrogel) in biomimetic hydrogels that did not contain an additional osteogenic signal and implanted for four weeks in calvarial defects of immunocompromised mice (**Figure 4A**). Comparable to the prospectively isolated, non-expanded cells e-BCSPs and e-SSCs formed bone nodules in the defect areas of the bone, as evaluated by μCT and histological analysis (**Figure 4B-D**). Additional GFP-specific stains revealed that both expanded cell types, comparable to prospectively isolated, non-expanded cells, localized to the margins of bone defects and actively participated in the formation of bone nodules by forming both osteoblasts and osteocytes (**Figure 4D**). These data indicate that e-SSCs and e-BCSPs (during the process of passaging and time in culture) retained their osteogenic potential but required additional effective osteogenic cues for the regeneration of large bone defects.

Low-dose BMP-2 enables e-SSCs and e-BCSPs mediated bone regeneration

Using BMP-2 doses below a critical threshold for bone regeneration fails likely due to insufficient local availability of osteogenic signals, as well as, osteogenic stem or progenitor cells (*45*). To assess whether low-dose BMP-2, which by itself is subcritical for bone formation, in presence of sufficient numbers of expanded osteogenic stem and progenitor cells could support bone regeneration, we encapsulated GFP$^+$ e-SSCs or e-BCSPs in biomimetic hydrogels (10^6 cells mL^{-1} / hydrogel) containing 0.2 μg BMP-2 and subsequently transplanted them into freshly created cranial defects (**Figure 4B**). μCT and histological analysis demonstrated that in presence of low-dose BMP-2, both e-SSCs and e-BCSPs promoted bone regeneration with an efficiency comparable to prospectively isolated, non-expanded BCSPs (**Figure 4B-D**). In contrast, control experiments revealed that low-dose BMP-2 in presence of mEFs could not promote bone regeneration (**Figure 4B**).

Moreover, GFP-specific stains confirmed that implanted e-SSCs and e-BCSPs directly contributed to newly formed bones, accumulated in bone structures of endosteal regions, and localized within fully matured bone, indicating their ability to differentiate into osteoblasts and osteocytes (**Figure 4D**). Together these data suggest that e-SSCs and e-

BCSPs retained their osteogenic properties and that both cell types in combination with subcritical doses of BMP-2 can efficiently participate in bone regeneration.

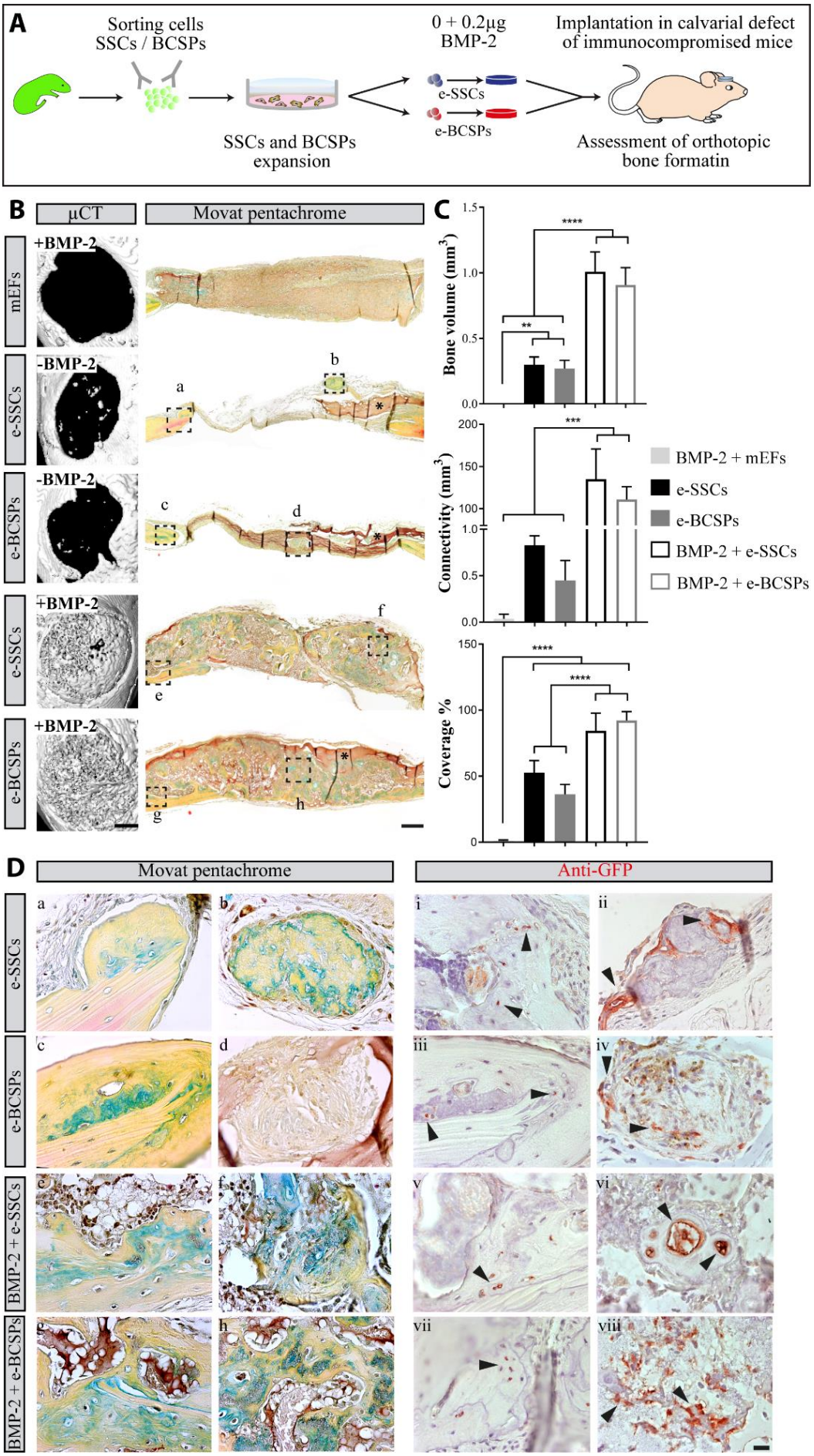
A
Sorting cells
SSCs / BCSPs
SSCs and BCSPs
expansion
0 + 0.2µg
BMP-2
e-SSCs
e-BCSPs
Implantation in calvarial defect
of immunocompromised mice
Assessment of orthotopic
bone formatin
B
µCT
Movat pentachrome
mEFs
+BMP-2
e-SSCs
-BMP-2
e-BCSPs
-BMP-2
e-SSCs
+BMP-2
e-BCSPs
+BMP-2
a
b
c
d
e
f
g
h
C
Bone volume (mm3)
Connectivity (mm3)
Coverage %
BMP-2 + mEFs
e-SSCs
e-BCSPs
BMP-2 + e-SSCs
BMP-2 + e-BCSPs
D
Movat pentachrome
Anti-GFP
e-SSCs
e-BCSPs
BMP-2 + e-SSCs
BMP-2 + e-BCSPs
i
ii
iii
iv
v
vi
vii
viii

Figure 4. *In vivo* osteogenic differentiation of expanded SSCs and BCSPs in orthotopic bone regeneration. (A) GFP^+ P3 limbs and sternum derived SSCs and BCSPs were expanded under standard cell culture conditions and encapsulated in PEG hydrogels (10^6 cells mL^{-1}/ hydrogel) containing 0 and 0.2μg BMP-2 before their implantation into calvarial defects of immunocompromised receiver mice. **(B)** 4-weeks post-craniotomy bone formation and localization of transplanted cells were assessed *ex situ*. Representative top views of 3D surface rendered μCT measurements for the transplanted cell populations (scale bar: 2 mm, left panel) along with Movat pentachrome stained sections of coronal cross sections [scale bar: 200μm, middle panel, red (fibrin) indicates muscle/vascularized tissue; yellow (reticular fibers/collagen) indicates bone; green/blue (mucin) indicates cartilaginous tissue; and black, nuclei and elastic fibers]. **(C)** Quantitative assessment of generated bone volume, connectivity and coverage. Data is depicted as mean ± SD. One-way ANOVA Bonferroni's post hoc test * $p < 0.05$, ** $p < 0.01$ *** $p < 0.001$, **** $p < 0.0001$. **(D)** Contribution of e-SSCs and e-BCSPs to newly formed calvarial bone was assessed by immunohistochemistry. **(a-h)** Inlets of coronal cross pentachrore stained sections. **(i-viii)** Anti-GFP immunohistochemistry for localization of $SSCs^+$ and $BCSPs^+$ to newly formed calvarial bone (scale bar: 20μm, black triangles indicate stained cells in osteocyte position within the remodeling healing area, asterisks indicate the remaining volume of the cell-trap).

Discussion

Our study shows that the combination of low-dose BMP-2 and a sufficient high number of skeletal stem or progenitor cells enable the efficient healing of bone defects, while the treatment with either cells alone or low-dose BMP-2 remains ineffective. In the natural healing sequence of bone defects, it is challenging to dissect the effect of an osteogenic cue from the contribution of the mobilized skeletal stem and progenitor cell populations. Here, we employed biomimetic hydrogel niches to study the recruitment of endogenous SSCs and BCSPs as well as to locally deliver them in presence or absence of the osteogenic growth factor BMP-2 and evaluate bone regeneration. These provisional hydrogel niches, which by enabling infiltration of healing associated cells can undergo remodeling, have already been shown to enable the regeneration of bone in presence of high-dose BMP-2 (*34*, *36*).

Bone regeneration requires BMP treatment that by far exceeds physiological doses in both mice and human patients (*46*, *47*). This could be due to the fact that delivered BMP either does not exert its full activity or that it does not encounter cellular entities which can promote or undergo osteogenesis (*48, 49*). Interestingly, biomimetic matrices-based of low-dose BMP-2 significantly improved the mobilization of SSCs and BCSPs as compared to control treatments, while at the same time it was subcritical to prompt bone regeneration. This suggests that in this healing microenvironment the low number of mobilized SSCs and BCSPs were insufficient to initiate bone formation. Additionally, it could also indicate that the BMP-2 delivery had vanished by the time osteogenic cells were recruited. Although high-dose BMP-2 more robustly mobilized SSCs and BCSPs, the efficient regeneration of bone defects could also be due to the improved availability of the osteogenic signal and therefore the enhanced differentiation of these cells (*48*).

Neonatal murine bone derived SSCs or BCSPs when transplanted beneath the renal capsule induced the formation of bone and bone marrow or bone, cartilage, and stromal cells, respectively (*32*). Therefore, we reasoned that the bone-healing microenvironment could provide sufficiently strong osteogenic cues to enable a purely cell mediated bone healing. In fact, in vicinity of regenerating bones, both SSCs and BCSPs spontaneously formed osteoblasts and even further differentiated into osteocytes. However, by the transplantation of 10^5 SSCs or 10^6 BCSPs comprising $0.5x10^3$ or $2x10^3$ colony forming unit (CFU-F) per mL of hydrogel, only very few small cartilage or bone nodules were formed

inside the treated bone defects. This is consistent with earlier findings, where the number of colony forming units (CFU-F) of human bone marrow derived mesenchymal stem cells (BM-MSCs) or adipose derived stem cells (hASCs) was shown to be a factor determining the bone forming potential of cell seeded scaffolds (*50, 51*). Together this suggests, that within such healing microenvironment SSCs and BCSPs can spontaneously differentiate into osteogenic cells, but for bone-formation would need to be present either in extremely high densities or further enriched in CFU-Fs.

Upon combined treatment of bone defects with prospectively isolated BCSPs and low-dose BMP-2 we observed robust bone formation. Additionally, the progeny of the transplanted BCSPs gave rise to osteoblasts and osteocytes within the regenerated bone (*42*). This data shows that subcritical doses of BMP-2 are sufficient to heal bone defects when bone progenitor cells are enriched at the site of bone healing. It also indicates that most efficient bone regeneration treatments should rely on the mobilization or transplantation of skeletal stem or progenitor cells, as well as, the release of adequate doses of osteogenic cues in a temporally controlled fashion (*52, 53*).

Prospectively isolated SSCs and BCSPs were assessed with intermediate expansion steps which according to previous studies, might lead to selective expansion of cellular entities due to paracrine effects or culture-induced phenotypic changes (*54*). By prospective isolation, the rare SSC and BCSP populations are difficult to obtain in sufficient quantities, limiting the utility of this approach for routine *in vivo* transplantation studies. Therefore, we aimed at expanding these cell populations, while evaluating the often-described cell culture-associated loss of phenotypic properties and cell type-specific functions. Indeed, the tested cell type specific marker expression (CD105 and CD200) changed very early (after two passages) during the *in vitro* expansion, resulting especially in a shift of a large fraction of SSCs into a phenotype more resembling to BCSPs. These data are consistent with earlier findings showing the partial loss of SSCs stem cell properties under standard *in vitro* culture (*32*). However, *in vitro* assays revealed that both cell culture expanded (4-6 passages) e-SSCs and e-BCSPs retained their osteogenic properties. Transplantations to the bone-healing microenvironment confirmed that both e-SSCs and e-BCSPs maintained their ability to spontaneously form osteogenic cells and regenerate bone in presence of low-dose BMP-2. These data indicate that e-SSCs and e-BCSPs represent specific endogenous healing associated stem cell populations. Therefore, these cells could be

highly relevant for the study of healing dynamics, cellular and molecular functions both *in vitro* and *in vivo*.

The herein used soft biomimetic hydrogels (30–250 Pa) are fully engineered substrates, which are specifically tailorable by modular formulation of biological functionalities with synthetic polymers (*34*). The flexibility of this system allows the adjustment of proteolytic degradability, integrin interactions as well as growth factor binding and release (*33, 34*). We are convinced that in combination with the e-SSCs and e-BCSPs this system enables the establishment of 3D culture models where individual healing parameters can be studied in the absence of confounding matrix signaling as would be the case for naturally derived biomaterials. More importantly, we propose that such models could be used to carefully evaluate the functionality of matrix immobilized signals by tuning their sequential release as it would be highly compelling to design novel healing promoting materials and treatment regimen. Finally, the properties of the newly developed materials could be directly tested in animal models and by this allow the correlation between *in vitro* and *in vivo* observation to further enable the efficient improvement of biomaterials.

While we showed that in vicinity of healing bones SSCs and BCSPs spontaneously differentiate to osteogenic cells, we have not systematically evaluated the influence of cell and CFU-F density at the site of healing. In light of the decreased mobilization and differentiation capacity of SSCs and BCSPs in aged or diabetic animals (*40, 55, 56*) this will be an important parameter for the establishment of clinically relevant models. In accordance with the diamond principle (*24*), it is expected that parameters for healing are interrelated as paracrine and/or autocrine signaling among SSCs and their progeny may positively regulate their own expansion, shifting from a stem population to a progenitor state, or participate in lineage specification (*32*). Therefore, also the correlation of BMP-2 dosing and cell seeding density will need further careful evaluation. Additionally, while we have shown that culture expanded fetal bone derived cells had substantial osteogenic properties, their functional relation to prospectively isolated, wound derived or fetal bone derived cells needs to be elucidated in more detail to appraise the predictive value of the herein used cells and models.

Conclusions

Taken together, in this study we have employed a biomimetic scaffold-based approach to investigate the role of osteogenic differentiation, as well as mobilization of SSCs and BCSPs during bone regeneration. We provide evidence that both the augmentation of SSCs and BCSPs at the healing site, together with the low-dose osteogenic signals would most efficiently foster bone healing. Additionally, we show that e-SSCs and e-BCSPs are healing representing stem and progenitor cells, which due to their relatively easy access enable the establishment and optimization of novel skeletal stem and progenitor cell as well as innovative materials-based healing promoting strategies.

Materials and Methods

Formation of hydrogels: Matrix metalloprotease (MMP)-sensitive TG-PEG hydrogels that contained 50uM RGD were formed with a final dry mass content of 1.7% in Tris buffer (50 mM, pH 7.6) containing calcium chloride (50 mM) as previously described (*33, 37*). Briefly, FXIII (200 U mL^{-1}, Fibrogammin P, CSL Behring, Switzerland) was activated with thrombin (2 U mL^{-1}, Sigma–Aldrich, Switzerland) for 30 min at 37 °C and stored at −80 °C. Stoichiometrically balanced solutions of eight-arm PEG macromeres that were either functionalized with pending FXIII substrate peptides glutamine acceptor (8-PEG-Gln) or lysine-donor followed by a MMP-sensitive sequence (8-PEG-$MMP_{sensitive}$-Lys) were prepared in Tris buffer (50 mM, pH 7.6) and calcium chloride (50 mM). Prior to the initiation of the $FXIII_a$-mediated (10 U $FXII_a$ mL^{-1}) cross-linking indicated amounts of growth factors and cells were added to the precursor solutions. Disc-shaped hydrogels were formed by casting droplets of complete hydrogel formulations between two sterile hydrophobic glass microscopy slides (Sigma-Aldrich, SigmaCote) separated by 0.8 mm thick spacers, clamping with binder clips, and incubation at 37 °C for 20 min. Hydrogel discs were released from glass sides and transferred to cell culture medium or stored in humidified atmosphere until transplantation into cranial defects.

Animals: All animal research procedures were approved by the Animal Experimentation Committee of the Veterinary Office of the Canton of Zurich, Switzerland and followed the guidelines of the Swiss Federal Veterinary Office for the use and care of laboratory animals. The cranial defect model was performed using 8-9-week-old female Crl:NMRI-$Foxn1^{nu}$ mice (purchased from Charles River) or 8-9-week-old female wild-type C57BL/6 mice (purchased from Harlan). For the isolation of SSCs and BCSPs postnatal day 3 (P3) transgenic C57BL/6-Tg(UBC-GFP)30Scha/J mice (GFP-labelled mice) maintained in our laboratory were employed.

Calvarial defect healing model: TG-PEG hydrogels of 4.4 mm diameter (11µl) that contained 0, 0.2, or 1µg recombinant human BMP-2 (CHO cell derived, PeproTech), 10^5 to 10^6 cells mL^{-1}/ hydrogel, or combinations thereof were prepared (conditions are summarized in Table 1). Craniotomies (4mm diameter) were created in the parietal bones of the skull one on each side of the sagittal suture. Pre-formed hydrogel discs were placed in the cranial defect and the skin was closed with 6.0 Vicryl sutures (Ethicon). Mice were

sacrificed after 4-weeks of treatment when calvaria were excised and fixed overnight in 4% Formalin and stored in TBS before *ex vivo* end-point analysis by µCT and histology.

	No. of Defects	Implanted Cells	BMP-2 [µg/hydrogel]
FACS	5	-	0
	5	-	0.2
	5	-	1.0
µCT and Histology	2	prospectively isolated SSCs	0
	3	prospectively isolated BCSPs	0
	3	prospectively isolated BCSPs	0.2
	5	-	0
	2	mEFs	0
	2	mEFs	0.2
	5	expanded SSCs	0
	5	expanded SSCs	0.2
	5	expanded BCSPs	0
	5	expanded BCSPs	0.2

Table 1: Grouped conditions of treated mice.

Prospective isolation and flow cytometry analysis of SSCs and BCSPs: For the isolation of SSCs and BCSPs hydrogel implants were harvested from cranial defects after 8 days of treatment or from skeletal tissues (limbs and sternum), which were dissected from P3 GFP-labeled mice. All tissues were enzymatically digested in collagenase A (Sigma Aldrich) supplemented with DNase (Qiagen) in MEMα 1% (v/v) penicillin/streptomycin solution and incubated at 37 °C for 40 min under gentle agitation. After collagenase digestion and neutralization in FACS buffer (2% v/v fetal bovine serum in PBS pH 7.2, 1 mM EDTA), undigested materials were further dissociated by repeated gentle pipetting. Total dissociated tissues were filtered through 100 µm nylon mesh, resulting cell suspensions centrifuged at 400 g at 4 °C and re-suspended in FACS buffer. Red blood cells were lysed by incubation with RBC lysis buffer for 10 min on ice before cells were washed and re-suspended in FACS buffer. Cells were stained with fluorochrome-conjugated antibodies against CD45 (Biolegend, cat.no 103105), Tie2 (Biolegend, cat.no 124007), AlphaV integrin (Biolegend, cat.no 104103), CD105 (Biolegend, cat.no 120411), CD90.2 (Biolegend, cat.no. 140309), 6C3 (Biolegend, cat.no. 108307) and CD200 (eBioscience, cat.no. 46-5200-80) for 30 min at 4 °C and fractioned by FACS. Sytox Red dead cell stain (ThermoFisher, cat.no. S34859) was used according to manufacturer instructions to evaluate cell viability. Flow cytometric analysis and sorting were performed on the BD FACSAria III (BD Biosciences) instruments using BD FACSDiva software. For cell sorting

100 μm nozzle and 20 psi sheath pressure were applied. Gates were defined according to the fluorescence intensity of the FMO containing the isotype control conjugated to the same fluorochrome as the primary antibodies. Data was further analyzed using FlowJo software (FlowJo LLC).

Micro-CT analysis of mouse calvarial specimens: Micro-CT scans of Formalin fixed calvaria were performed with a Micro-CT40 (Scanco Medical AG) the X-ray tube operating at an energy of 70 kVp and an intensity of 114 μA reconstructing three-dimensional images with an isotropic voxel size of 10 μm. A global threshold corresponding to 9.8% of the maximum grey values was used to separate bone from surrounding soft tissues. Regions of interest for the evaluation were selected by placing a cylinder of 3 mm diameter in the center of bone defects. Bone volume, connectivity, and trabecular thickness within this mask were measured using the ImageJ plugin BoneJ (*38*). Bone coverage was measured in a dorso-ventral projection of the cylindrical mask.

Histological staining and immunohistochemistry of orthotopic bone formation*:* Formalin fixed calvaria were completely decalcified with 10% w/v EDTA (pH 7.14) and embedded in paraffin. For histological evaluations, 4 μm thin tissue sections were stained with stained with hematoxylin & eosin (Sigma-Aldrich) and Movat pentachrome. Briefly for Movat pentechrome, sections were sequentially incubated with alcian blue (Fluka, 1g in 100 ml 1% glacial acetic acid) for 10 min, alkaline alcohol (10% v/v Ammonium hydroxide in 95% EtOH) for 1 hour, Weigert's iron hematoxylin (Weigert reagent A and B in a ratio 1:1) for 20 minutes, brilliant crocein R-fuchsine (1 part Biebrich Scarlet-Acid Fuchsin [SIGMA Art.Nr:HT151] and 1 part 0.2% acidic fuchsin in 0.5% acetic acid) for 20 minutes, 0.5% acetic acid for 30 seconds 5% PWS (5% phosphortungsten acid; cantonal pharmacy Zurich) 15 min, 0.5% acetic acid for 2 minutes, washed 3 times with absolute ethanol for 5 minutes, saffron du grâtinais dye (6g Safran pouder in 100 ml absolute EtOH) overnight incubation and mounted in Eukit (Kindler GmbH, Freiburg Germany). If not stated otherwise intermediate washing steps were conducted with H_20. In Movat pentachrome, red (fibrin) indicates muscle/vascularized tissue; yellow (reticular fibers/collagen) indicates bone; green/blue (mucin) indicates cartilaginous tissue; and black, nuclei and elastic fibers. For immunohistochemical localization of GFP implanted cells in orthotopic bone formation, sections were exposed to anti-GFP antibody (Abcam, cat. no. ab290) overnight at 4°C. Next, they were incubated with a biotinylated secondary goat anti-rabbit antibody for 1 hour at room temperature, followed by incubation with an

avidin-biotin-peroxidase complex for 1 hour at room temperature, according to manufacturer's instructions (Vector Laboratories Inc., PK-6101). Peroxidase was revealed by incubation with AEC (3-amino-9-ethylcarbazole) red substrate (Vector Laboratories Inc., SK-4200) prior blocking with 3% H_2O_2.

CFU-F assay: Prospectively isolated SSCs and BCSPs (110 cells cm^{-2}) were seeded on collagen-coated wells (Techno Plastic Products) and cultured for 9 days in MEMα containing 10% (v/v) FCS and 1% (v/v) P/S at 37 °C with 5 % CO_2. After fixation with 4 % paraformaldehyde for 20 min, colonies were stained with 0.05 % (w/v) crystal violet solution for 30 min. Cell clusters counting > 30 cells, were scored as colony.

Cell culture: SSCs and BCSPs populations were seeded on collagen coated plates and cultured in maintenance medium consisting of minimal essential medium alpha (MEMα, Gibco Life Technologies), 10% (v/v) fetal calf serum (FCS, Gibco Life Technologies) and 1% (v/v) penicillin/streptomycin solution (P/S, Gibco Life Technologies) under standard culture conditions (37 °C with 5 % CO_2). K41 (wild-type) mouse embryonic fibroblasts were maintained in Dulbecco's modified eagle medium (DMEM-low glucose, with Glutamax; Gibco Life Technologies), supplemented with 20% FCS and 1% v/v P/S as previously described (*39*). MC3T3-E1 sc24 were maintained in MEMα with 10% (v/v) FCS and 1% (v/v) P/S. All cells were used between passage 2 and 6.

Osteogenic differentiation in 2D culture: To assess their osteogenic differentiation cells were seeded at 3000 cells cm^{-2} density (n=4) and cultured for 8 days in the respective maintenance medium which was supplemented only with 0 or 100ng mL^{-1} BMP-2. After removal of the cell culture medium cells were washed twice with PBS. For alkaline phosphatase (ALP) staining cells incubated with alkaline phosphatase (ALP) substrate solution (prepared from FAST BCIP/NBT tablets; Sigma-Aldrich, Switzerland) as recommended by the manufacturer. When visually sufficient color had developed in positive controls (8 min), the substrate solution in all conditions was replaced with PBS and cells were imaged with a Zeiss 200M inverted microscope. To measure ALP activity, cells were collected in 500 µL lysis buffer (0.56 M 2-amino-2-methyl-1-propanol, 0.2% Triton X-100, pH 10 in H_2O) and gently triturated by repeated pipetting. The cell lysate was centrifuged for 10 min. at 13000 rpm before the supernatant was collected. ALP substrate (20 mM 4-nitrophenyl phosphate disodium salt hexahydrate, 4 mM $MgCl_2$ in lysis buffer) was added to the cell lysates in a 96-well plate and incubated at 37 °C for 10

min. before absorbance was measured at 410 nm with a microplate reader. ALP activity measurements were normalized on the relative DNA content that was measured in cell lysates by the CyQuant NF cell proliferation assay kit (Molecular Probes).

Osteogenic differentiation in 3D culture using Alizarin Red Staining: Cells were encapsulated in TG-PEG hydrogels (1.7% PEG, 50 µM RGD) at final concentration of 5 * 10^6 mL^{-1} (n=4), and cultured in maintenance medium or osteogenic induction medium consisting of Dulbecco's Modified Eagle Medium (DMEM) high glucose (Gibco Life Technologies) with 10 % (v/v) FCS and 1 % (v/v) P/S modified with 10 mM HEPES, 1 mM sodium pyruvate, 2 mM L-glutamine, L-ascorbic acid (50 µg mL^{-1}), 10 mM β-glycerol phosphate and 100ng mL^{-1} BMP-2. The medium was changed every 3-4 days. Hydrogels were fixed with 4% paraformaldehyde for 20 min, washed with water, and stained for 20 min with Alizarin Red S (40 mM) in ddH_2O (pH 4.1, adjusted with 0.1% NH_4OH) under gentle agitation. After extensive washing with water, hydrogels were imaged with a Zeiss 200M inverted microscope. For colorimetric quantification Alizarin Red S was extracted by incubating hydrogels with 10% (v/v) acetic acid in ddH2O at RT for 30 min under gentle agitation. The extracted was collected, incubated at 85 °C for 10 min, and kept in ice for 5 min. The resulting slurry was centrifuged at 13000 rpm for 15 min, 500 µL of the supernatant was transferred to a new 1.5 mL microcentrifuge tube where the pH was adjusted within the range of 4.1 - 4.5 before the absorbance was measured at 405 nm with a microplate reader.

qRT-PCR analysis of 3D cultured cells: To determine their osteogenic in 3D culture cells were encapsulated in TG-PEG hydrogels (1.7% PEG, 50 µM RGD) at a final concentration of 3 * 10^6 mL^{-1} (n=4). Cultured were conducted for 8 days in MEMα with 10% (v/v) FCS and 1% (v/v) P/S supplemented with 0 and 100ng mL^{-1} BMP-2 at 37 °C with 5 % CO_2. Medium and growth factors were replaced once. Cells were harvested by digesting the hydrogels with collagenase A (2mg mL^{-1}) for 30 min at 37 °C followed by 10 min centrifugation at 13000 rpm and RT. Total RNA was isolated from cell pellets by the RNeasy Micro Kit (Qiagen) according to the manufacturer's instructions. For quantitative real-time PCR (qRT-PCR) 80 ng RNA were converted into 22 µl cDNA by means of the High-Capacity cDNA Reverse Transcription Kit (Applied Biosystems). qRT-PCR was carried out using TaqMan Universal PCR Master Mix (Applied Biosystems) and the ViiA™ 7 Real-Time PCR System (Applied Biosystems). The following TaqMan primer/probe sets were used for gene expression tests: Mm00475834_m1 (Alpl); Mm04209856_m1 (Sp7).

Values were normalized to Mm02619580_g1 (Actb) mRNA levels and presented as fold change according to the $2^{-\Delta\Delta CT}$ method.

***Statistical Analysis**:* All statistical analysis was performed in GraphPad Prism (GraphPad Software). Data analysis was performed using one or two-way ANOVA and post Bonferroni's correction or Student's *t*-test assuming two-tailed distribution and unequal variances. In all cases, a *p*-value of < 0.05 was considered statistically significant, and all data is depicted as mean ± SD (S.D).

Acknowledgements

We thank Dr. Paolo Cinelli for support with micro-CT, Dr. Flora Nicholls for help with animal experiments, Dr. Chafik Ghayor for providing MC3T3-E1 sc24 cells. The research leading to these results has received funding from the People Programme (Marie Curie Actions) of the European Union's Seventh Framework Programme FP7/2007-2013/ under REA grant agreement No. 607868 (iTERM).

References

1. E. J. Carragee, E. L. Hurwitz, B. K. Weiner, A critical review of recombinant human bone morphogenetic protein-2 trials in spinal surgery: emerging safety concerns and lessons learned. *Spine J* **11**, 471-491 (2011).
2. L. F. Charles, J. L. Woodman, D. Ueno, G. Gronowicz, M. M. Hurley, L. T. Kuhn, Effects of low dose FGF-2 and BMP-2 on healing of calvarial defects in old mice. *Exp Gerontol* **64**, 62-69 (2015).
3. J. N. Zara, R. K. Siu, X. Zhang, J. Shen, R. Ngo, M. Lee, W. Li, M. Chiang, J. Chung, J. Kwak, B. M. Wu, K. Ting, C. Soo, High doses of bone morphogenetic protein 2 induce structurally abnormal bone and inflammation in vivo. *Tissue Eng Part A* **17**, 1389-1399 (2011).
4. R. A. D. Carano, E. H. Filvaroff, Angiogenesis and bone repair. *Drug Discovery Today* **8**, 980-989 (2003).
5. Z. S. Ai-Aql, A. S. Alagl, D. T. Graves, L. C. Gerstenfeld, T. A. Einhorn, Molecular Mechanisms Controlling Bone Formation during Fracture Healing and Distraction Osteogenesis. *Journal of Dental Research* **87**, 107-118 (2008).
6. L. C. Gerstenfeld, D. M. Cullinane, G. L. Barnes, D. T. Graves, T. A. Einhorn, Fracture healing as a post-natal developmental process: Molecular, spatial, and temporal aspects of its regulation. *Journal of Cellular Biochemistry* **88**, 873-884 (2003).
7. X. Wang, Y. Wang, W. Gou, Q. Lu, J. Peng, S. Lu, Role of mesenchymal stem cells in bone regeneration and fracture repair: a review. *International orthopaedics* **37**, 2491-2498 (2013).
8. D. L. Worthley, M. Churchill, J. T. Compton, Y. Tailor, M. Rao, Y. Si, D. Levin, M. G. Schwartz, A. Uygur, Y. Hayakawa, S. Gross, B. W. Renz, W. Setlik, A. N. Martinez, X. Chen, S. Nizami, H. G. Lee, H. P. Kang, J. M. Caldwell, S. Asfaha, C. B. Westphalen, T. Graham, G. Jin, K. Nagar, H. Wang, M. A. Kheirbek, A. Kolhe, J. Carpenter, M. Glaire, A. Nair, S. Renders, N. Manieri, S. Muthupalani, J. G. Fox, M. Reichert, A. S. Giraud, R. F. Schwabe, J. P. Pradere, K. Walton, A. Prakash, D. Gumucio, A. K. Rustgi, T. S. Stappenbeck, R. A. Friedman, M. D. Gershon, P. Sims, T. Grikscheit, F. Y. Lee, G. Karsenty, S. Mukherjee, T. C. Wang, Gremlin 1 identifies a skeletal stem cell with bone, cartilage, and reticular stromal potential. *Cell* **160**, 269-284 (2015).
9. E. Ratcliffe, K. E. Glen, M. W. Naing, D. J. Williams, Current status and perspectives on stem cell-based therapies undergoing clinical trials for regenerative medicine: case studies. *Br Med Bull* **108**, 73-94 (2013).
10. M. Mumme, A. Barbero, S. Miot, A. Wixmerten, S. Feliciano, F. Wolf, A. M. Asnaghi, D. Baumhoer, O. Bieri, M. Kretzschmar, G. Pagenstert, M. Haug, D. J. Schaefer, I. Martin, M. Jakob, Nasal chondrocyte-based engineered autologous cartilage tissue for repair of articular cartilage defects: an observational first-in-human trial. *The Lancet* **388**, 1985-1994.
11. L. Duplomb, M. Dagouassat, P. Jourdon, D. Heymann, Concise review: embryonic stem cells: a new tool to study osteoblast and osteoclast differentiation. *Stem Cells* **25**, 544-552 (2007).
12. M. Dominici, K. Le Blanc, I. Mueller, I. Slaper-Cortenbach, F. Marini, D. Krause, R. Deans, A. Keating, D. Prockop, E. Horwitz, Minimal criteria for defining multipotent mesenchymal stromal cells. The International Society for Cellular Therapy position statement. *Cytotherapy* **8**, 315-317 (2006).
13. V. Tollemar, Z. J. Collier, M. K. Mohammed, M. J. Lee, G. A. Ameer, R. R. Reid, Stem cells, growth factors and scaffolds in craniofacial regenerative medicine. *Genes & Diseases* **3**, 56-71 (2016).
14. S. Sundelacruz, D. L. Kaplan, Stem cell- and scaffold-based tissue engineering approaches to osteochondral regenerative medicine. *Seminars in cell & developmental biology* **20**, 646-655 (2009).
15. S. Bose, M. Roy, A. Bandyopadhyay, Recent advances in bone tissue engineering scaffolds. *Trends Biotechnol* **30**, 546-554 (2012).
16. F. J. O'Brien, Biomaterials & scaffolds for tissue engineering. *Materials Today* **14**, 88-95 (2011).
17. B. Dhandayuthapani, Y. Yoshida, T. Maekawa, D. S. Kumar, Polymeric Scaffolds in Tissue Engineering Application: A Review. *International Journal of Polymer Science* **2011**, 1-19 (2011).
18. A. Raic, L. Rodling, H. Kalbacher, C. Lee-Thedieck, Biomimetic macroporous PEG hydrogels as 3D scaffolds for the multiplication of human hematopoietic stem and progenitor cells. *Biomaterials* **35**, 929-940 (2014).
19. E. S. Place, J. H. George, C. K. Williams, M. M. Stevens, Synthetic polymer scaffolds for tissue engineering. *Chemical Society Reviews* **38**, 1139-1151 (2009).

20. S. Stratton, N. B. Shelke, K. Hoshino, S. Rudraiah, S. G. Kumbar, Bioactive polymeric scaffolds for tissue engineering. *Bioactive Materials* **1**, 93-108 (2016).
21. N. R. Patel, A. K. Whitehead, J. J. Newman, M. E. Caldorera-Moore, Poly(ethylene glycol) Hydrogels with Tailorable Surface and Mechanical Properties for Tissue Engineering Applications. *ACS Biomaterials Science & Engineering*, (2016).
22. T. A. Einhorn, The Cell and Molecular Biology of Fracture Healing. *Clinical Orthopaedics and Related Research* **355**, S7-S21 (1998).
23. L. Claes, S. Recknagel, A. Ignatius, Fracture healing under healthy and inflammatory conditions. *Nature reviews. Rheumatology* **8**, 133-143 (2012).
24. P. V. Giannoudis, T. A. Einhorn, D. Marsh, Fracture healing: The diamond concept. *Injury* **38**, S3-S6 (2007).
25. H. Ito, Chemokines in mesenchymal stem cell therapy for bone repair: a novel concept of recruiting mesenchymal stem cells and the possible cell sources. *Mod Rheumatol* **21**, 113-121 (2011).
26. B. Sacchetti, A. Funari, S. Michienzi, S. Di Cesare, S. Piersanti, I. Saggio, E. Tagliafico, S. Ferrari, P. G. Robey, M. Riminucci, P. Bianco, Self-renewing osteoprogenitors in bone marrow sinusoids can organize a hematopoietic microenvironment. *Cell* **131**, 324-336 (2007).
27. S. Mendez-Ferrer, T. V. Michurina, F. Ferraro, A. R. Mazloom, B. D. Macarthur, S. A. Lira, D. T. Scadden, A. Ma'ayan, G. N. Enikolopov, P. S. Frenette, Mesenchymal and haematopoietic stem cells form a unique bone marrow niche. *Nature* **466**, 829-834 (2010).
28. D. Park, Joel A. Spencer, Bong I. Koh, T. Kobayashi, J. Fujisaki, Thomas L. Clemens, Charles P. Lin, Henry M. Kronenberg, David T. Scadden, Endogenous Bone Marrow MSCs Are Dynamic, Fate-Restricted Participants in Bone Maintenance and Regeneration. *Cell Stem Cell* **10**, 259-272 (2012).
29. P. Bianco, X. Cao, P. S. Frenette, J. J. Mao, P. G. Robey, P. J. Simmons, C. Y. Wang, The meaning, the sense and the significance: translating the science of mesenchymal stem cells into medicine. *Nat Med* **19**, 35-42 (2013).
30. P. Bianco, P. G. Robey, Skeletal stem cells. *Development* **142**, 1023-1027 (2015).
31. M. Kassem, P. Bianco, Skeletal stem cells in space and time. *Cell* **160**, 17-19 (2015).
32. C. K. Chan, E. Y. Seo, J. Y. Chen, D. Lo, A. McArdle, R. Sinha, R. Tevlin, J. Seita, J. Vincent-Tompkins, T. Wearda, W. J. Lu, K. Senarath-Yapa, M. T. Chung, O. Marecic, M. Tran, K. S. Yan, R. Upton, G. G. Walmsley, A. S. Lee, D. Sahoo, C. J. Kuo, I. L. Weissman, M. T. Longaker, Identification and specification of the mouse skeletal stem cell. *Cell* **160**, 285-298 (2015).
33. M. Ehrbar, S. C. Rizzi, R. G. Schoenmakers, B. S. Miguel, J. A. Hubbell, F. E. Weber, M. P. Lutolf, Biomolecular hydrogels formed and degraded via site-specific enzymatic reactions. *Biomacromolecules* **8**, 3000-3007 (2007).
34. M. Ehrbar, A. Sala, P. Lienemann, A. Ranga, K. Mosiewicz, A. Bittermann, S. C. Rizzi, F. E. Weber, M. P. Lutolf, Elucidating the role of matrix stiffness in 3D cell migration and remodeling. *Biophys J* **100**, 284-293 (2011).
35. P. S. Lienemann, S. Metzger, A. S. Kivelio, A. Blanc, P. Papageorgiou, A. Astolfo, B. R. Pinzer, P. Cinelli, F. E. Weber, R. Schibli, M. Behe, M. Ehrbar, Longitudinal in vivo evaluation of bone regeneration by combined measurement of multi-pinhole SPECT and micro-CT for tissue engineering. *Sci Rep* **5**, 10238 (2015).
36. M. P. Lutolf, F. E. Weber, H. G. Schmoekel, J. C. Schense, T. Kohler, R. Muller, J. A. Hubbell, Repair of bone defects using synthetic mimetics of collagenous extracellular matrices. *Nat Biotechnol* **21**, 513-518 (2003).
37. M. Ehrbar, S. C. Rizzi, R. Hlushchuk, V. Djonov, A. H. Zisch, J. A. Hubbell, F. E. Weber, M. P. Lutolf, Enzymatic formation of modular cell-instructive fibrin analogs for tissue engineering. *Biomaterials* **28**, 3856-3866 (2007).
38. M. Doube, M. M. Klosowski, I. Arganda-Carreras, F. P. Cordelieres, R. P. Dougherty, J. S. Jackson, B. Schmid, J. R. Hutchinson, S. J. Shefelbine, BoneJ: Free and extensible bone image analysis in ImageJ. *Bone* **47**, 1076-1079 (2010).
39. K. Nakamura, A. Zuppini, S. Arnaudeau, J. Lynch, I. Ahsan, R. Krause, S. Papp, H. De Smedt, J. B. Parys, W. Muller-Esterl, D. P. Lew, K. H. Krause, N. Demaurex, M. Opas, M. Michalak, Functional specialization of calreticulin domains. *J Cell Biol* **154**, 961-972 (2001).
40. O. Marecic, R. Tevlin, A. McArdle, E. Y. Seo, T. Wearda, C. Duldulao, G. G. Walmsley, A. Nguyen, I. L. Weissman, C. K. Chan, M. T. Longaker, Identification and characterization of an injury-induced skeletal progenitor. *Proceedings of the National Academy of Sciences of the United States of America* **112**, 9920-9925 (2015).
41. R. Tevlin, E. Y. Seo, O. Marecic, A. McArdle, X. Tong, B. Zimdahl, A. Malkovskiy, R. Sinha, G. Gulati, X. Li, T. Wearda, R. Morganti, M. Lopez, R. C. Ransom, C. R. Duldulao, M. Rodrigues, A. Nguyen, M. Januszyk, Z. Maan, K. Paik, K.-S. Yapa, J. Rajadas, D. C. Wan, G. C. Gurtner,

M. Snyder, P. A. Beachy, F. Yang, S. B. Goodman, I. L. Weissman, C. K. F. Chan, M. T. Longaker, Pharmacological rescue of diabetic skeletal stem cell niches. *Science Translational Medicine* **9**, (2017).

42. C. K. F. Chan, P. Lindau, W. Jiang, J. Y. Chen, L. F. Zhang, C.-C. Chen, J. Seita, D. Sahoo, J.-B. Kim, A. Lee, S. Park, D. Nag, Y. Gong, S. Kulkarni, C. A. Luppen, A. A. Theologis, D. C. Wan, A. DeBoer, E. Y. Seo, J. D. Vincent-Tompkins, K. Loh, G. G. Walmsley, D. L. Kraft, J. C. Wu, M. T. Longaker, I. L. Weissman, Clonal precursor of bone, cartilage, and hematopoietic niche stromal cells. *Proceedings of the National Academy of Sciences of the United States of America* **110**, 12643-12648 (2013).
43. D. H. Kempen, L. Lu, T. E. Hefferan, L. B. Creemers, A. Maran, K. L. Classic, W. J. Dhert, M. J. Yaszemski, Retention of in vitro and in vivo BMP-2 bioactivities in sustained delivery vehicles for bone tissue engineering. *Biomaterials* **29**, 3245-3252 (2008).
44. W. Y. Baek, Y. J. Kim, B. de Crombrugghe, J. E. Kim, Osterix is required for cranial neural crest-derived craniofacial bone formation. *Biochem Biophys Res Commun* **432**, 188-192 (2013).
45. C. M. Cowan, T. Aghaloo, Y. F. Chou, B. Walder, X. Zhang, C. Soo, K. Ting, B. Wu, MicroCT evaluation of three-dimensional mineralization in response to BMP-2 doses in vitro and in critical sized rat calvarial defects. *Tissue Eng* **13**, 501-512 (2007).
46. V. Agrawal, M. Sinha, A review on carrier systems for bone morphogenetic protein-2. *J Biomed Mater Res B Appl Biomater*, (2016).
47. M. Ronga, A. Fagetti, G. Canton, E. Paiusco, M. F. Surace, P. Cherubino, Clinical applications of growth factors in bone injuries: Experience with BMPs. *Injury* **44, Supplement 1**, S34-S39 (2013).
48. J. D. Boerckel, Y. M. Kolambkar, K. M. Dupont, B. A. Uhrig, E. A. Phelps, H. Y. Stevens, A. J. García, R. E. Guldberg, Effects of protein dose and delivery system on BMP-mediated bone regeneration. *Biomaterials* **32**, 5241-5251 (2011).
49. H. Uludag, T. Gao, T. Porter, W. Friess, J. Wozney, Delivery Systems for BMPs: Factors Contributing to Protein Retention at an Application Site. *Journal of Bone & Joint Surgery* **83**, S128-S135 (2001).
50. A. M. Müller, A. Mehrkens, D. J. Schäfer, C. Jaquiery, S. Güven, M. Lehmicke, R. Martinetti, I. Farhadi, M. Jakob, A. Scherberich, I. Martin, Towards an intraoperative engineering of osteogenic and vasculogenic grafts from the stromal vascular fraction of human adipose tissue. *European Cells and Materials* **19**, 127-135 (2010).
51. T. Walenda, G. Bokermann, M. S. Ventura Ferreira, D. M. Piroth, T. Hieronymus, S. Neuss, M. Zenke, A. D. Ho, A. M. Muller, W. Wagner, Synergistic effects of growth factors and mesenchymal stromal cells for expansion of hematopoietic stem and progenitor cells. *Exp Hematol* **39**, 617-628 (2011).
52. M. N. Knight, K. D. Hankenson, Mesenchymal Stem Cells in Bone Regeneration. *Advances in Wound Care* **2**, 306-316 (2013).
53. D. Sheyn, S. Ben-David, G. Shapiro, S. De Mel, M. Bez, L. Ornelas, A. Sahabian, D. Sareen, X. Da, G. Pelled, W. Tawackoli, Z. Liu, D. Gazit, Z. Gazit, Human Induced Pluripotent Stem Cells Differentiate Into Functional Mesenchymal Stem Cells and Repair Bone Defects. *Stem Cells Transl Med* **5**, 1447-1460 (2016).
54. J. J. Bara, R. G. Richards, M. Alini, M. J. Stoddart, Concise Review: Bone Marrow-Derived Mesenchymal Stem Cells Change Phenotype Following In Vitro Culture: Implications for Basic Research and the Clinic. *STEM CELLS* **32**, 1713-1723 (2014).
55. A. Stolzing, E. Jones, D. McGonagle, A. Scutt, Age-related changes in human bone marrow-derived mesenchymal stem cells: consequences for cell therapies. *Mech Ageing Dev* **129**, 163-173 (2008).
56. O. Katsara, L. G. Mahaira, E. G. Iliopoulou, A. Moustaki, A. Antsaklis, D. Loutradis, K. Stefanidis, C. N. Baxevanis, M. Papamichail, S. A. Perez, Effects of donor age, gender, and in vitro cellular aging on the phenotypic, functional, and molecular characteristics of mouse bone marrow-derived mesenchymal stem cells. *Stem Cells Dev* **20**, 1549-1561 (2011).

Supplementary data

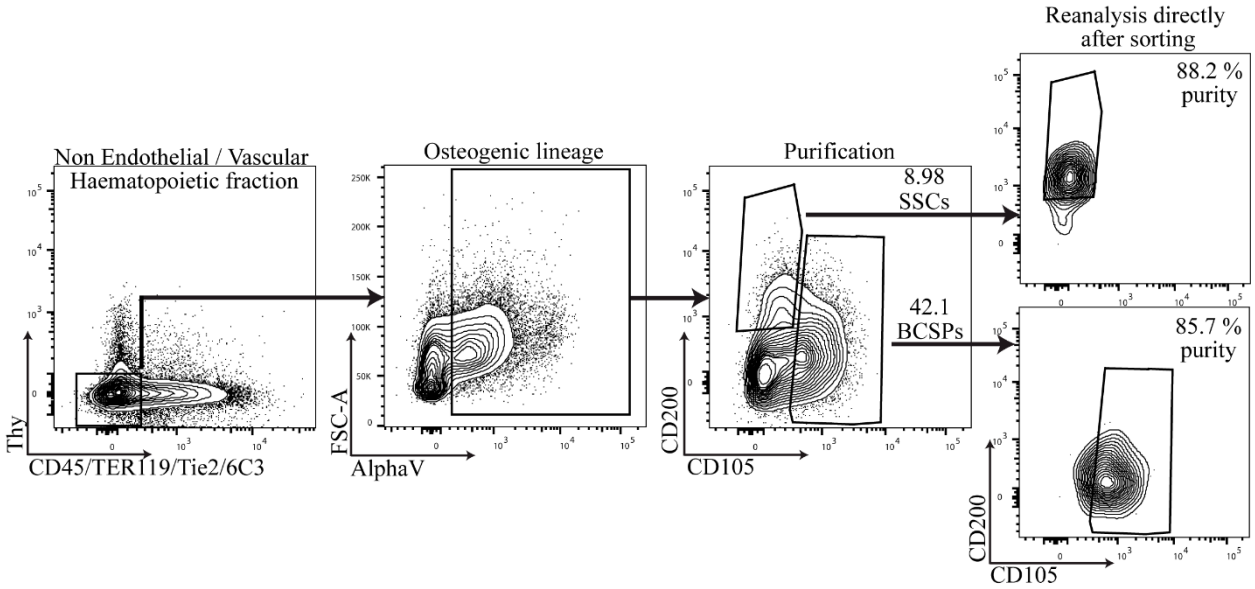

Figure S1. FACS gating strategy for isolation of SSCs and BCSPs. Cells were isolated from limbs and sternum digestion of GFP$^+$ mice at P3 and stained for flow cytometry. Representative FACS analysis of SSCs [CD45$^-$Ter-119$^-$Tie2$^-$AlphaV$^+$Thy$^-$6C3$^-$CD105$^-$CD200$^+$] and of BCSPs [CD45$^-$Ter-119$^-$Tie2$^-$AlphaV$^+$Thy$^-$6C3$^-$CD105$^+$] purified from pre-gated live, GFP$^+$, singlet cells. Representative analysis of post-sort purity for SSCs (top right) and BCSPs (bottom right) is shown.

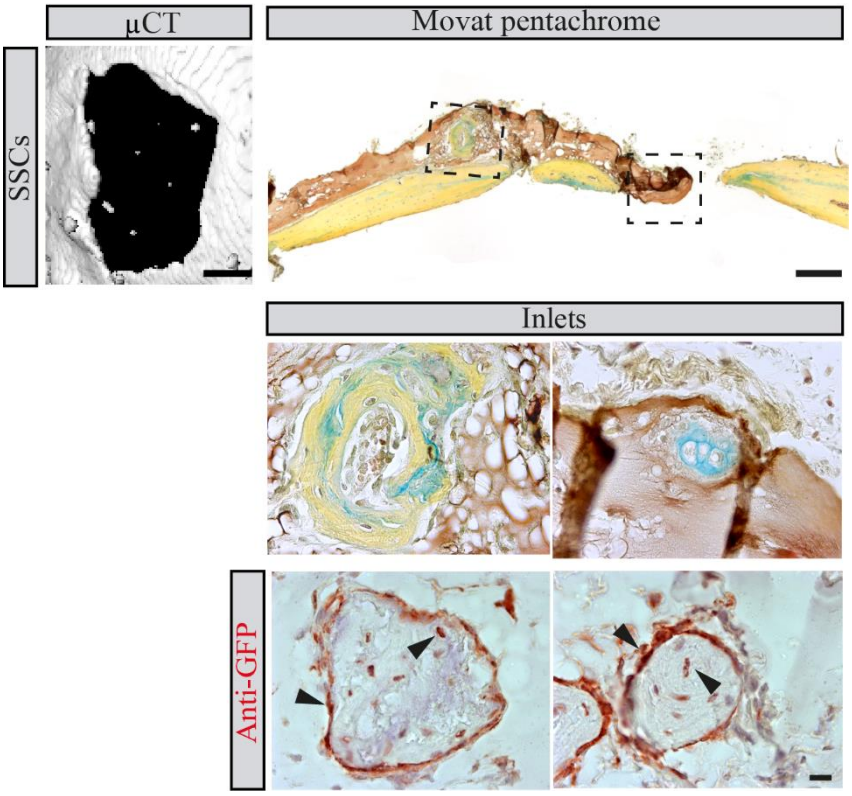

Figure S2. *In vivo* osteogenic differentiation of prospectively isolated SSCs. 4-weeks post-craniotomy bone formation and localization of transplanted cells were assessed *ex situ*. Representative top views of 3D surface rendered µCT measurements for the SSCs (scale bar: 2 mm, left panel) along with Movat pentachrome stained sections of coronal cross sections [scale bar: 200 µm, middle panel, red (fibrin) indicates muscle/vascularized tissue; yellow (reticular fibers/collagen) indicates bone; green/blue (mucin) indicates cartilaginous tissue; and black, nuclei and elastic fibers]. Contribution of SSCs to newly formed

calvarial bone was assessed by immunohistochemistry. Inlets of coronal cross pentachrore stained sections. SSCs⁺ stained in anti-GFP at osteocyte position confirming their participation in bone nodule regeneration (scale bar: 20 µm, bottom panel black triangles indicate stained cells in osteocyte position in the remodeling healing area).

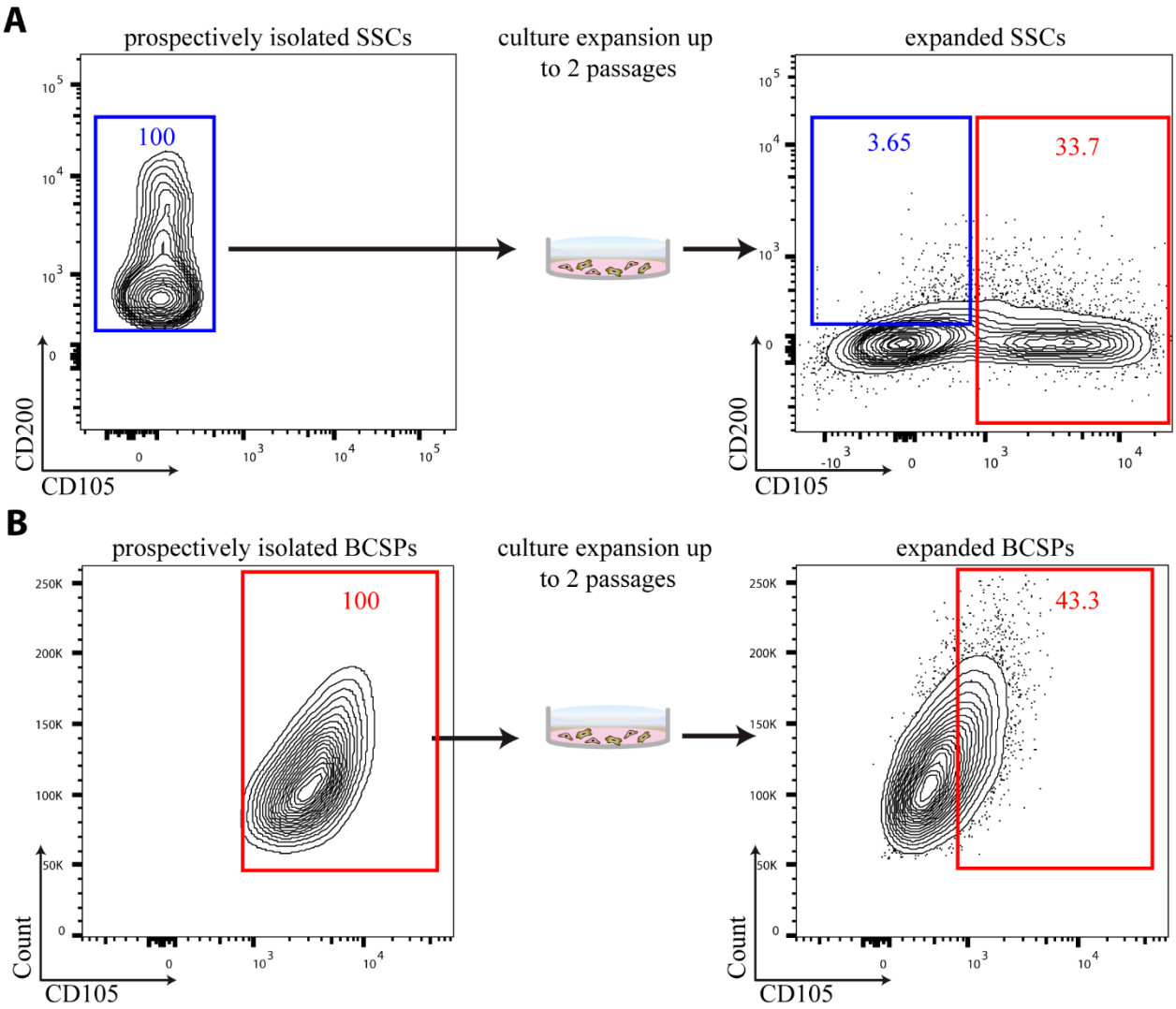

Figure S3. Shifting fates of SSCs and BCSPs upon culture expansion. (A) Prospectively isolated SSCs exhibit differential expression of CD105 and CD200 markers after culture expansion. **(B)** Expression of CD105 after culture expansion of prospectively isolated BCSPs. Cells were gated on live, GFP⁺, lineage negative, AlphaV⁺, singlets.

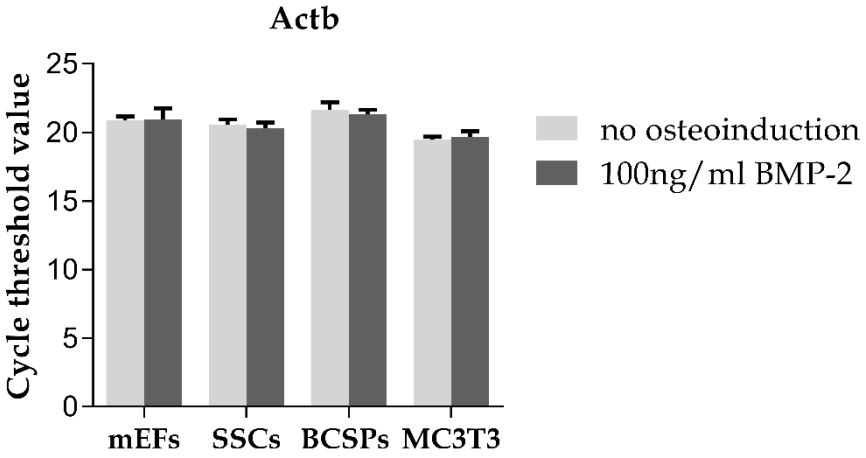

Figure S4. Actb distibution within the different subpopulations. No difference and an average CT mean of 20 fold increase was observed in presence of 0 (no osteoinduction) and 100 ng mL^{-1} BMP-2 (osteoinduction) treatment between the different subpopulations.